The Effect of Gravity Degradation on Low-Speed Centrifuge Capillary Pressure Data

Zhigang Andy Chen and Douglas W. Ruth
Dept. of Mechanical and Industrial Engineering,
University of Manitoba, Winnipeg, Manitoba, Canada R3T 2N2

The gravity degradation effect has been identified as a significant physical problem in using centrifuge techniques for determining capillary pressure curves. In 1992, the authors characterized the effect by an angle; however, such an evaluation is simplistic. Here, a new model is constructed to characterize the effect quantitatively. The results with simulated data sets show that there exists a pronounced effect of gravitation on the horizontal centrifugal field in low-speed experiments ($\leq$ 500 rpm on a standard Beckman centrifuge). Gravity affects the production history for some samples, which leads to inaccurate interpretations of capillary pressure information near the threshold pressure.

Introduction

Capillarity is the dominant phenomenon in multiphase flow through a porous medium. Capillarity is usually characterized as capillary pressure vs. a phase saturation (or phase content) relationship. Capillary pressure relationships have long been a major topic in porous-material-related disciplines, such as soil science and petroleum engineering. Capillary pressure and relative permeability are two particularly important parameters required by reservoir engineers in order to calculate the production performance of oil and gas reservoirs. Although there are other techniques available for the experimental determination of these properties, the centrifuge technique provides a very useful tool.

In the centrifuge method for determining capillary pressure, a core sample plug, initially saturated with one fluid, is spun around a vertical axis. The capillary pressure at a cross section of the sample counterbalances the pressure difference between coexisting fluids caused by the centrifuge acceleration field. The sample is spun at various angular speeds ω and the amount of production of one of the fluid pairs is recorded. A relationship between capillary pressure and phase saturation can be calculated from the data set, the angular rotation speeds ω, and the produced volumes of one fluid $\overline{V}$.

The fundamental idea, the apparatus design, and the interpretation technique of centrifuge capillary pressure can be traced back to the pioneering contribution of Hassler and Brunner in 1945. In the last four decades, the centrifuge technique has been widely used throughout the core-analysis industry. However, there are still many problems associated with the fundamental assumptions on which this method is based, despite the progress made in data interpretation techniques, which are rooted in Hassler and Brunner's one-dimensional simplified model. In principle, this model assumes a one-dimensional centrifugal force field. Christiansen and Cerise (1987) and Christiansen (1992) realized the possible errors of the one-dimensional model and developed a two-dimensional model to account for the radial centrifugal field distribution. They found systematic errors due to this effect. Ayappa et al. (1989) also discussed models for arbitrary-shaped core samples, and they derived the relevant governing equations. They gave two models in particular for core plugs shaped as cylinders and slabs. However, no one has yet considered in detail the possible effect of gravitation.

The gravitation problem stems from the traditional design of centrifuge rotors. The most common centrifuge used for capillary pressure and relative permeability measurement is made by Beckman. There are several problems with this centrifuge: (1) it has a horizontal rotor head, and the sample is exposed to the effects of gravity at low speeds; (2) the sample is located close to the center of rotation, which leads to large changes in centrifugal acceleration along the axis of the sample, which in turn leads to difficulties in interpreting the experimental data; (3) the centrifuge does not have adequate speed control at low speeds, which results in either no data or very poor data for samples that have low capillary pressures, especially those used for soil sample experiments; and

(4) both manual and automatic data collection systems rely on optical readings to determine the amount of wetting component production. As far as points (1) and (3) are concerned, gravitational acceleration is expected to play a role in routine laboratory experiments. Gravitational acceleration leads to a total acceleration field that is not purely centrifugal. This effect is referred to as "gravity degradation," in the present article. It is generally postulated that gravity degradation occurs in high permeability and porosity core-sample experiments where low angular speeds are used initially. Core plugs in the rotor are usually spun in a horizontal plane, and the centrifugal force is also assumed to be acting horizontally (perpendicular to the vertical rotational axis). In reality, because of the gravitational acceleration of the earth, where the rotating centrifugal field and the earth's gravitational field are at right angles, the true force acting on a fluid particle inside a core plug will be "dragged down," creating an inclined acceleration force field. Ruth and Chen (1992) were the first to discuss this problem. In order to characterize the effect, they used an angle α

$$\alpha = \tan^{-1}\left(\frac{g}{\omega^2 r}\right). \tag{1}$$

However this angle does not give any quantitative information on the effect on capillary pressure curves. In the present article, a three-dimensional model is developed that directly describes the effect of gravity degradation.

Theory

If we assume that a centrifuge rotor is spinning around a vertical axis $O-Z$ at an angular speed ω, any fluid particle in a core plug, which is confined in the rotor, will also be in rotation at the same ω around the axis $O-Z$, as shown in Figure 1. According to the d'Alembert principle (Li, 1990), which states that the forces acting on any particle of a fluid are considered to be in a state of equilibrium when the rotating particle is subjected to a body force in a form not only of earth gravity but also centrifugal acceleration, if we assume P is the pressure of a particle of a fluid at any location, the differential pressure is

$$dP = \rho\omega^2 x\,dx - \rho\omega^2 y\,dy - \rho g\,dz, \tag{2}$$

for a Cartesian coordinate system, or

$$dP = \rho\omega^2 r\,dr - \rho g\,dz, \tag{3}$$

for a horizontally radial coordinate system. Integrating Eq. 3 results in

$$P = \frac{1}{2}\rho\omega^2 r^2 - \rho g z + C. \tag{4}$$

Defining a reference point allows us to determine C in the previous equation. The rotating centrifugal force field with an earth gravity effect can be visualized as a paraboloid of revolution. Let $A(r_0)$ be an equipressure surface inside the sample, where r_0 is the radial distance to the upper point where $A(r_0)$ intersects the top surface of the sample. As the radius r_0 increases, $A(r_0)$ is generated as a result of the intersecting process of the paraboloid of rotation with the core-plug cylinder, as shown in Figure 1. The intersection starts at point I (the *first touch*) and ends at point J or at point K, depending on how serious the gravity effect becomes (at point J or K it can be imagined as the *last touch*). For such equipressure surfaces, there must exist an integral $\int_{r_{0min}}^{r_{0max}} A(r_0)\,dr_0$, which yields the volume of the core plug, $\pi R^2(r_{outlet} - r_{inlet}) = V$, where r_{inlet} and r_{outlet} are defined in Figure 1. The saturation material balance equation is established by $A(r_0)$ by means of the following equation:

$$\bar{S}_w = \frac{1}{V}\int_{r_{0min}}^{r_{0max}} S_w(P_c)A(r_0)\,dr_0 \tag{5}$$

where r_{0min} and r_{0max} are the two limiting boundaries, which we will detail later.

To solve Eq. 5, a particular expression for $A(r_0)$ is needed. In order to determine this expression for the equipressure surface, Eq. 3 must be used. An equipressure surface is described by $dP = 0$, or

$$\rho\omega^2 r\,dr = \rho g\,dz. \tag{6}$$

Integrating,

$$\frac{1}{2}\omega^2(r^2 - r_0^2) = g(z - z_0), \tag{7}$$

where (r, z) and (r_0, z_0) are any two points on the equipressure surface. Equation 7 describes clearly the three-dimensional force-field distribution: not only a radial centrifugal field, but a vertical gravitational acceleration is acting as shown in Figures 2a and 2b. Because of the vertically acting

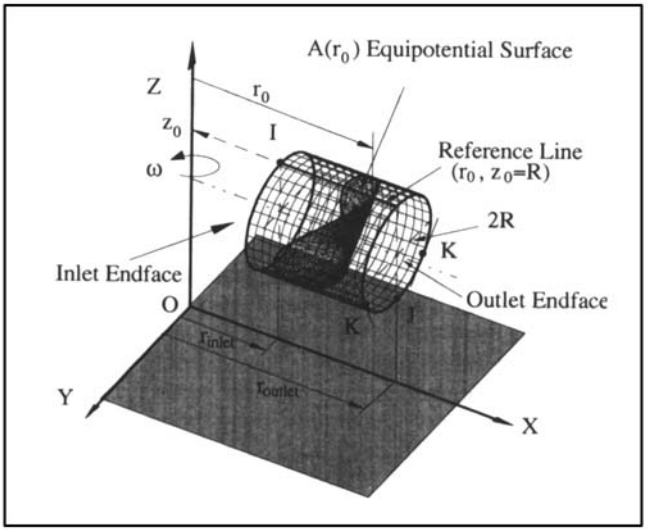

Figure 1. Three-dimensional centrifugal field.

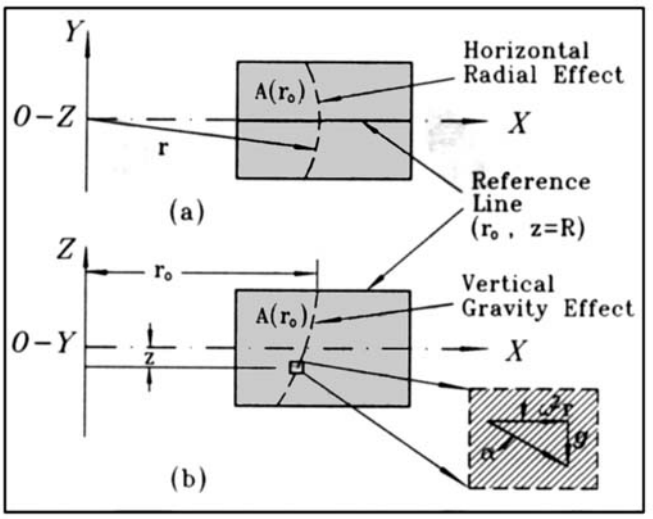

Figure 2. Inclined centrifuge field: radial and gravity effects.

(a) Top view; (b) lateral view.

gravitational acceleration, the centrifugal field is dragged down, leading to the creation of an inclined angle α, which is defined in Eq. 1. As the rotation speed ω increases, the effect of g becomes negligible, that is, $\alpha = 0$, and the capillary pressure is counterbalanced by a pure, horizontal centrifugal force. When $\omega = 0$, $\alpha \to 90°$, and the capillary pressure is related only to the vertical gravitational acceleration field. When initiating an experiment with a centrifuge, there is always a combined distribution of both horizontal centrifugal and vertical gravitational fields, and the inclination of the distribution is strongly dependent on the rotation speeds used during the experiment. At low speed stages for an experimental run, gravitational acceleration plays a significant role in *distorting* the pressure distribution.

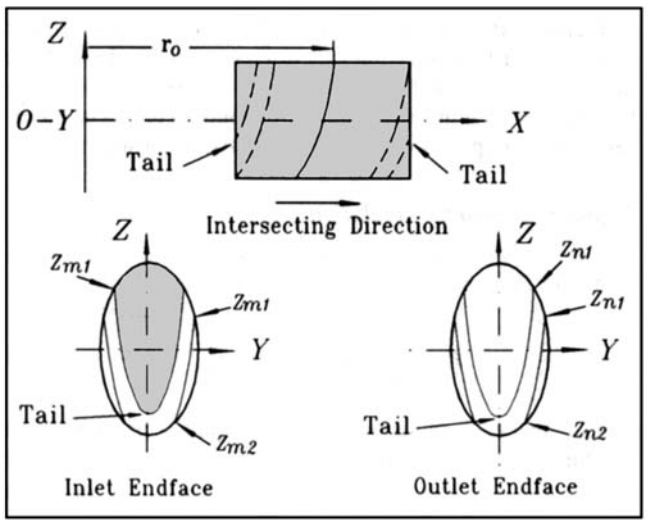

Figure 3. Intersecting process of paraboloid and cylinder.

Although this is obviously a three-dimensional problem, the equipotential surface can be treated using two-dimensional considerations by eliminating one of the three variables. We will define (r, z) as any point inside the core sample plug, and select (r_0, z_0) at the top line of the core sample plug. We then have $z_0 = R$, as shown in Figure 1. This condition is imposed because we assume that the initial pressure distribution in the cross section of the core sample is hydrostatic. Accordingly, if we define $C_g = 2g/\omega^2$, Eq. 7 can be rewritten as

$$r^2 = x^2 + y^2 = r_0^2 + C_g(z - R) \tag{8}$$

or

$$x^2 = r_0^2 - y^2 + C_g(z - R). \tag{9}$$

It follows that $x = f(y, z)$ for the equipotential surface that passes through the point $r = r_0$, $z = z_0$. Therefore we can write

$$A(r_0) = \int\int F(x, y, z)\, dz\, dy \tag{10}$$

where $F(x, y, z) = \sqrt{1 + f_y^2 + f_z^2}$, and $f_y = \partial x/\partial y$, $f_z = \partial x/\partial z$ (Thomas, 1960).

Equipotential surfaces

If r_0 is used (for convenience, we use x instead of r_0 in a Cartesian system) as the linear distance reference from the axis of rotation to locations on the top line of the core plug cylinder, then when performing the integration of Eq. 5, one has to separate the integrand for different ranges of r_0 in order to account for the distribution of equipotential surfaces inside the core plug. Here r_0 is equivalent to the r in Christiansen's case (1992). The range of r_0 is divided into several zones, depending on different combinations of the parameters involved in the problem. Generally, when $C_g \le 2R$, there are five zones (surface intersects edge of the inner endface at two locations; surface intersects edge of the inner endface at four locations; surface does not intersect endfaces; surface intersects the edge of the outer face at four locations; and surface intersects the edge of the outer face at two locations) as illustrated in Figure 3 and

$$r_{\text{inlet}} \le r_0 \le \sqrt{r_{\text{inlet}}^2 + 2RC_g} \qquad \text{for zone 1,}$$

$$\sqrt{r_{\text{inlet}}^2 + 2RC_g} \le r_0 \le \sqrt{R^2 + r_{\text{inlet}}^2 + RC_g + \frac{C_g^2}{4}} \qquad \text{for zone 2,}$$

$$\sqrt{R^2 + r_{\text{inlet}}^2 + RC_g + \frac{C_g^2}{4}} \le r_0 \le r_{\text{outlet}} \qquad \text{for zone 3,}$$

$$r_{\text{outlet}} \le r_0 \le \sqrt{r_{\text{outlet}}^2 + 2RC_g} \qquad \text{for zone 4}$$

and

$$\sqrt{r_{\text{outlet}}^2 + 2RC_g} \le r_0$$

$$\le \sqrt{R^2 + r_{\text{outlet}}^2 + RC_g + \frac{C_g^2}{4}} \qquad \text{for zone 5.}$$

Therefore,

$$r_{0\min} = r_{\text{inlet}}$$

and

$$r_{0\max} = \sqrt{R^2 + r_{\text{outlet}}^2 + RC_g + C_g^2/4}$$

for this situation. Therefore, r_{inlet} corresponds to the *first touch* of the "paraboloid" with the core plug "cylinder," and r_{outlet} corresponds to the *last touch* of the "paraboloid" with the "cylinder." In Figure 3, when we look at the two endfaces, we can get a better understanding of these zones. At the inlet endface, the darker hatched upper portion is the projection of the equipotential surface inside the core plug for zone 1, and the tail of this portion arrives at the bottom of the endface when this zone ends. During the first zone intersecting process, the "paraboloid" always has two junction points in the upper portion of the endface circle. As the intersection goes on, we start the second zone, and the projection of the equipotential surface will cover both the darker and less dark hatched upper portions until the projection covers the whole endface circle. The projection of all equipotential surfaces in zone 3 will cover the whole inlet endface. This zone starts when r_0 arrives at the right top point of the outlet endface, and the projection of equipotential surface under consideration reflected in the outlet endface is the lower, darker hatched portion; thereafter, it is followed by zone 5, which lasts until the shape of the equipotential surface in the outlet endface totally disappears.

When $C_g \ge 2R$, only three zones are observed

$$r_{\text{inlet}} \le r_0 \le \sqrt{r_{\text{inlet}}^2 + 2RC_g} \qquad \text{for zone 1,}$$

$$\sqrt{r_{\text{inlet}}^2 + 2RC_g} \le r_0 \le r_{\text{outlet}} \qquad \text{for zone 2,}$$

and

$$r_{\text{outlet}} \le r_0 \le \sqrt{r_{\text{outlet}}^2 + 2RC_g} \qquad \text{for zone 3.}$$

Therefore, $r_{0\min} = r_{\text{inlet}}$ and $r_{0\max} = \sqrt{r_{\text{outlet}}^2 + 2RC_g}$ for this situation. Determination of the integral boundaries is covered in the Appendix, where the definition and the determination of the junction points, z_{m1}, z_{n2}, z_{n1}, z_{n2}, are also explained (combining with Figure 3). The integrand $F(x, y, z) = \sqrt{1 + f_y^2 + f_z^2}$ contains two derivatives:

$$f_y = \frac{\partial x}{\partial y} = \frac{1}{2} \frac{-2y}{\sqrt{r_0^2 - y^2 + C_g(z - R)}} \qquad (11)$$

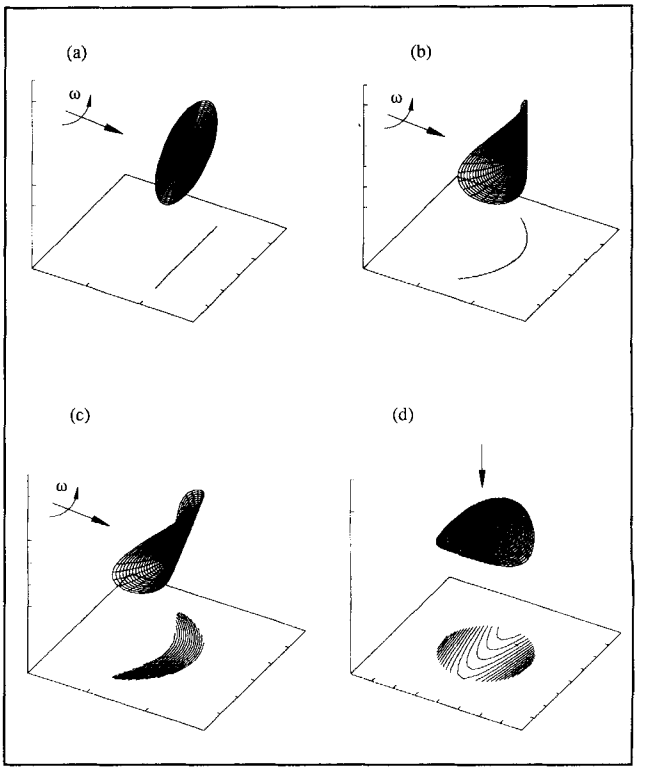

Figure 4. Equipotential surfaces for different cases.

(a) One-dimensional linear case; (b) two-dimensional radial case; (c) three-dimensional gravity effect (plan); (d) three-dimensional gravity effect (elevation).

and

$$f_z = \frac{\partial x}{\partial z} = \frac{1}{2} \frac{C_g}{\sqrt{r_0^2 - y^2 + C_g(z - R)}}. \qquad (12)$$

Figure 4 gives several pictures of the equipotential surfaces for one-, two-, and three-dimensional cases. Because C_g characterizes the extent of gravity degradation, it can be seen in Figure 4 that the bottom portion of the surface tends to incline toward the rotating axis at elevated C_g values. A vertical "mask," resembling a beekeeper's mask, is found when $C_g = 0$, as shown in Figure 4b, corresponding to Christiansen's case, which depends on purely geometrical considerations.

Capillary pressure calculations

For capillary pressure considerations at boundaries, we can postulate that the capillary pressure at point I will be

$$P_{cI} = \frac{1}{2}\Delta\rho\omega^2(r_{0\max}^2 - r_{\text{inlet}}^2), \qquad (13)$$

and we also have to assume that the capillary pressure at the two tangent points K, located at the edge of the outside endface ($x = r_{\text{outlet}}$, $y = \pm\sqrt{R^2 - C_g^2/4}$, $z = -C_g/2$) or at the right bottom point J, are zero in Figure 1, or

$$P_{cK} = P_{cJ} = 0 \qquad (14)$$

for most cases of C_g values. When C_g is exceptionally large ($C_g > 2R$), the zero P_c boundary condition occurs at the bottom point J of the outside endface of the core-plug cylinder. The $r_{0\max}$, the maximum radius required for a zero-capillary pressure boundary, can be found through a detailed geometrical analysis. In our problem, when $C_g \le 2R$,

$$r_{0\max} = \sqrt{r_{\text{outlet}}^2 + R^2 + RC_g + \frac{C_g^2}{4}},$$

and when $C_g \ge 2R$, $r_{0\max} = \sqrt{r_{\text{outlet}}^2 + 2RC_g}$.

Capillary pressure at any point inside the core sample plug can be calculated using the following equation:

$$P_c(r, z) = \frac{1}{2}\Delta\rho\omega^2\left(r_{0\max}^2 - r^2 - C_g(R - z)\right). \quad (15)$$

For the purpose of performing the integration in Eq. 5, the capillary pressure at any point on the top line of the core cylinder is

$$P_c(r_0) = \frac{1}{2}\Delta\rho\omega^2(r_{0\max}^2 - r_0^2). \quad (16)$$

The standard value of gravity acceleration is 9.80665 m/s^2. For the low angular rotation speeds of 100, 200, and 300 (rpm), the values of the factor C_g (in cm) are 17.885, 4.471, 1.987, respectively. For these speeds, earth's gravitational acceleration plays an important role. As the rotation speed increases, the value of C_g becomes smaller and the correction term for gravity degradation becomes negligible. In this situation, the analysis reduces to Christiansen's case (Christiansen, 1992), a geometric consideration of rotating fields in which equipressure surfaces can be visualized as quadric surfaces being formed by the intersection of two cylinders. Further, if no core-plug geometry is considered, the situation will be again reduced, either to the fundamental case or to Hassler and Brunner's one-dimensional equation. These cases are given later in examples. Therefore, the present model represents a complete picture of the true force field distribution acting during centrifugation.

Gravity Effect

In this section, we address how gravitational acceleration affects the centrifuge experimental data.

Capillary pressure models

Equation 5 is a Volterra integral equation of the first kind, and is known to be strongly numerically unstable. It is very difficult, if not impossible, to find its explicit analytical solution because of its three-dimensional complexity. However, we can use implicit methods or parameter estimation techniques, assuming some explicit capillary pressure functional models, to quantify the error introduced in conventional one- or two-dimensional analyses (neglecting gravity effects). Available capillary pressure models include Bentsen's log and power models (Bentsen and Anli, 1977; Golaz and Bentsen, 1980), Corey's model (Corey, 1954), as well as Thomeer's model (Thomeer, 1960). These models can be used to test the effect of gravitational degradation on capillary pressure curves.

We chose one of Bentsen's capillary pressure models to show the significance of the problem. The choice is for illustrative purposes only. Other models show similar trends. Bentsen's log model is expressed as

$$S_w = \begin{cases} 1, & \text{when } P_c \le P_t; \\ S_{wr} + (1 - S_{wr}) \exp\left(-\dfrac{P_c - P_t}{\sigma}\right), & \text{when } P_c \ge P_t \end{cases} \quad (17)$$

where P_t is the threshold pressure, S_{wr} the irreducible connate water saturation, and σ the pressure span factor.

Synthesized data set

In order to examine and quantify the effect of gravitational acceleration on the centrifuge experimental data, synthesized data sets have been constructed. Concerning the capillary pressure just discussed vs. the saturation model, we assume that the threshold pressure is zero and that the pressure span, σ, take the value of 0.05, 0.10, 0.125, 0.25, and 0.50 psi. These values are representative of high permeability ($k > 1$ darcies) and porosity ($\phi > 25\%$) sandstone sample experiments, including unconsolidated tar sand core samples. The density difference values are assumed to be 0.15, 0.85, and 1.01 g/cm^3, representing three experiments: oil–brine, oil–air, and air–brine. As used in Christiansen's paper (1992), the irreducible connate water saturation S_{wr} is selected as 0.2. The rotational speed (in rpm) data set includes 50, 100, 150, 200, 300, 400, 500, 600, 800, and 1,000 (for high permeability and porosity samples, the rpm schedule should include speeds from 150 to 500 rpm). The rotor and core plug system are assumed to be characterized by $r_{\text{inlet}} = 6.06$ cm, $r_{\text{outlet}} = 8.6$ cm, and $R = 1.27$ cm. These figures correspond to a 1.0-in.-long and 1.0-in.-dia. core sample, mounted in a rotor with an outer rotation distance of 8.6 cm. These numbers are typical for a Beckman centrifuge.

For capillary pressure calculations, we have three cases available: Hassler-Brunner's one-dimensional case, Christiansen's two-dimensional case, and the new three-dimensional case. The capillary pressure equations are as follows:

$$P_c(x) = 0.7953473 \times 10^{-7}\Delta\rho(\text{rpm})^2(r_{\text{outlet}}^2 - x^2) \quad (18a)$$

for the Hassler-Brunner equation;

$$P_c(x, y) = 0.7953473 \times 10^{-7}\Delta\rho(\text{rpm})^2(r_{\text{outlet}}^2 + R^2 - x^2 - y^2) \quad (18b)$$

for the Christiansen equation; and

$$P_c(x, y, z) = 0.7953473 \times 10^{-7}\Delta\rho(\text{rpm})^2 \times \left(r_{0\max}^2 - x^2 - y^2 - C_g(R - z)\right) \quad (18c)$$

for the new model, where $r_{0\max}$ is defined in the previous section.

Results and Discussion

Figure 5 shows capillary pressure curves for Bentsen's log model using the model parameters given previously. We are concerned with high permeability and porosity samples primarily with air–brine systems, for which we believe the gravity degradation effect plays an active role, and the capillary pressure curves, which exhibit the feature of very low values of σ.

Capillary pressure

Figure 6 shows the results for capillary pressures at a specified location (denoted by P_{c1}, Eq. 18c), which is a traditional part of the data set. For the Hassler-Brunner one-dimensional analysis, the capillary pressure at the whole inlet endface is assumed to have the same value, that is, P_{c1} is uniform everywhere on the inlet endface. Christiansen (1992) introduced a P_{c1} that occurs at the vertical center line (from the top to the bottom) of the inlet endface. For the three-dimensional consideration, the P_{c1} is located at the top point of the inlet endface (point I in Figure 2). Therefore, we have chosen the P_{c1} from Eq. 18c as the reference value that makes the most sense for the practical situations in Figure 6. Figure 6 shows the changes of saturation for the P_{c1}'s for various density differences. The three-dimensional values are always located above the one- and two-dimensional values, while Hassler-Brunner's one-dimensional values are always less than the others. When the rotation speed exceeds 500 rpm, the three-dimensional values converge on Christiansen's two-dimensional values, because above this speed the effect of C_g vanishes and the three-dimensional model is identical to Christiansen's theory. Christiansen's model does not include the gravity effect, and from the curves it can be seen that his lines are basically equivalent to Hassler-Brunner's solutions at low speed. Neither Ayappa et al. (1989) nor Christiansen (1992) studied data interpretation for the low speed zone in their studies.

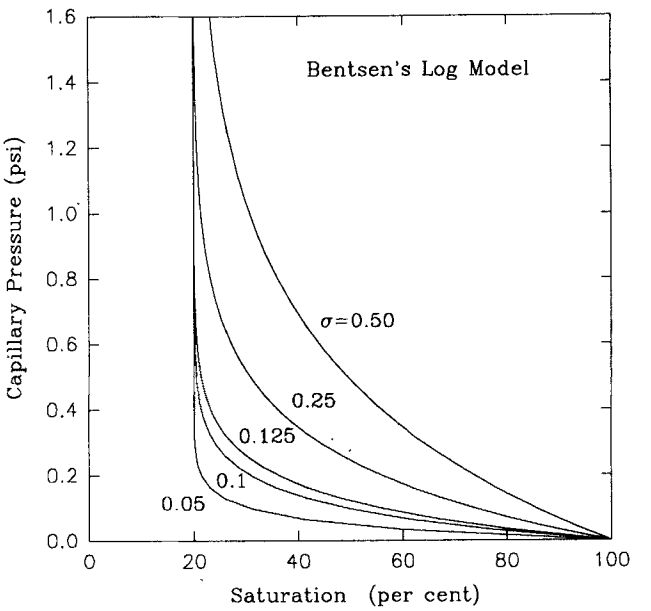

Figure 5. Capillary pressure curves for Betsen log model.

Production behavior

Equation 5 was used to test the significance of the gravitational acceleration. The Gauss-Legendre algorithm (Maron, 1982) was used to numerically evaluate the triple integral. Grid refining tests were carried out using from 10 to 76 points in the Gauss-Legendre algorithm, and sufficient precision was obtained (Stroud and Secrest, 1966). All computations were run using double precision on a SunFortran system.

Figures 7 to 11 give the results for simulated data sets. The rpm is plotted vs. the produced fluid or the mean saturation in the core sample. Five σ values are shown to illustrate the significance of the effect under study. All the figures show the same trend at low speed—that gravitational acceleration has a pronounced effect on production behavior. A single capillary pressure vs. saturation relationship can be used to generate different production responses, depending on the model (one-dimensional, two-dimensional, or three-dimensional) assumed. The curves including the gravity effect (three-dimensional) represent the true production response. The trend implies that vertical gravitation reduces the whole centrifugal force field, leading to a variation in saturation. This is reflected particularly in the threshold zone where the gravity-included curves are lower than Christiansen's curves. In the data analysis process, a lower mean saturation value at the same capillary pressure results in lower saturation. The true capillary pressure curves for a real centrifugal force distribution should move toward a lower saturation than Christiansen's capillary pressure curve in the threshold zone, and, of course, lower than Hassler-Brunner's curve. From Figures 7 to 11 it is found that the two data sets diverge below a speed of approximately 500 rpm, and that the discrepancies can be as great as 10 percentage points of saturation when the speed is 100 rpm.

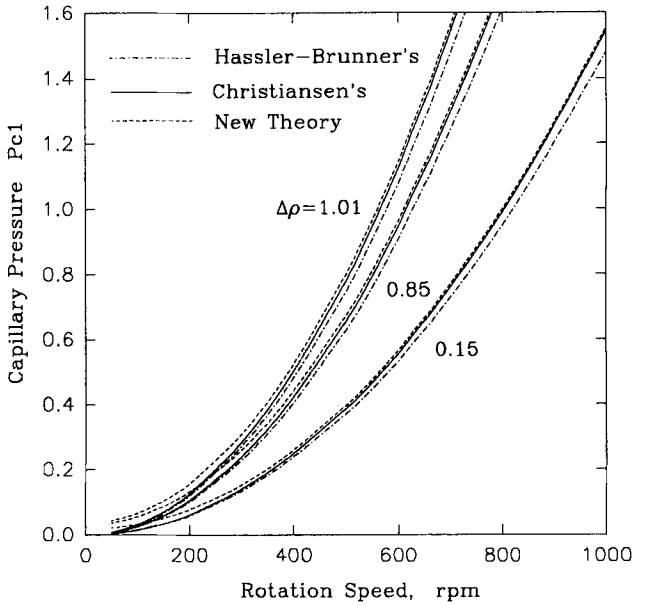

Figure 6. Reference capillary pressure Pc1.

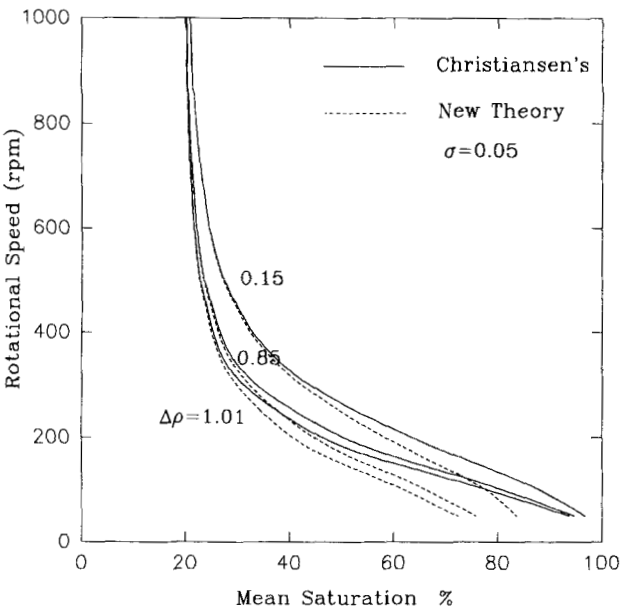

Figure 7. Production histories generated with two theories.

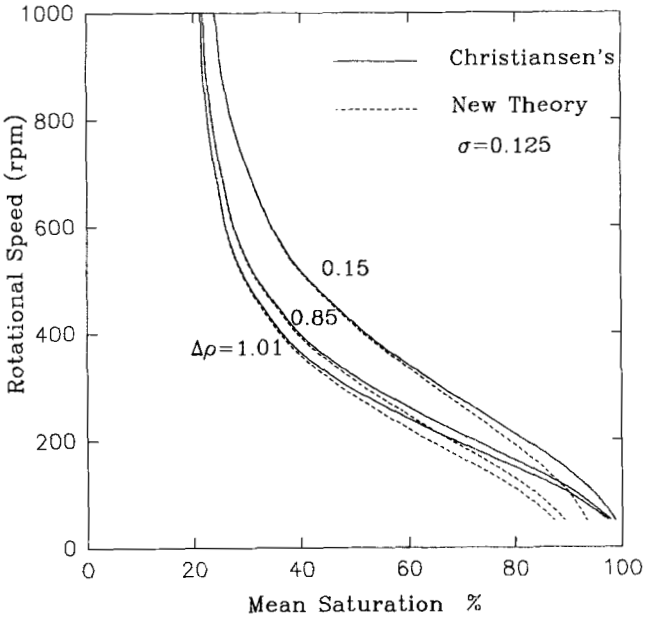

Figure 9. Production histories generated with two theories.

The largest effect occurs in samples with the lowest σ and the greatest density difference. In this study, the synthesized data for the extreme case are given in Figure 7. When σ is 0.5 psi (Figure 11), the effect is diminished. Previous authors have attributed disagreement between centrifuge and porous plate data to the neglect of radial effects (Christiansen, 1992; Forbes et al., 1994). We now might argue that this disagreement is caused in part by the fact that in a centrifuge experiment the gravity effect has not been properly accounted for.

Data interpretations

We have identified a significant effect on experimental centrifuge capillary pressure data introduced by gravitational acceleration for high permeability and porosity samples (especially for unconsolidated tar sands, as well as soil samples), which exhibit a capillary pressure characteristic of very low pressure span σ values. For low permeability samples, such an effect contributes little to data quality, because of the high rpm required. However, the effect does have an in-

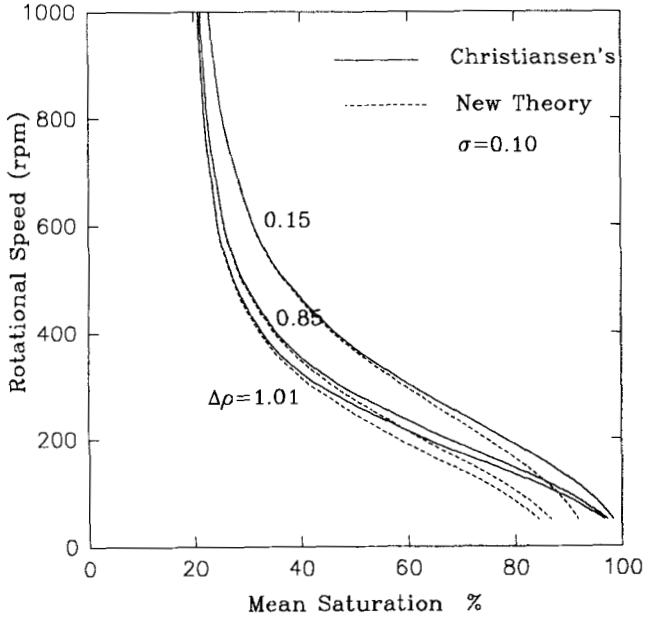

Figure 8. Production histories generated with two theories.

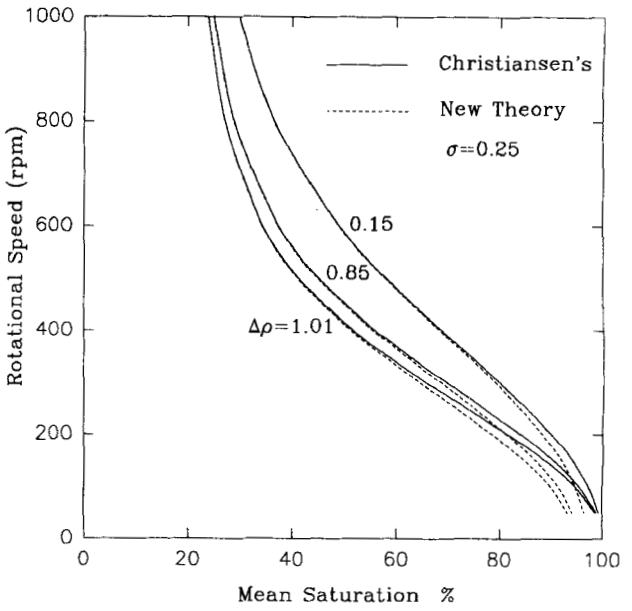

Figure 10. Production histories generated with two theories.

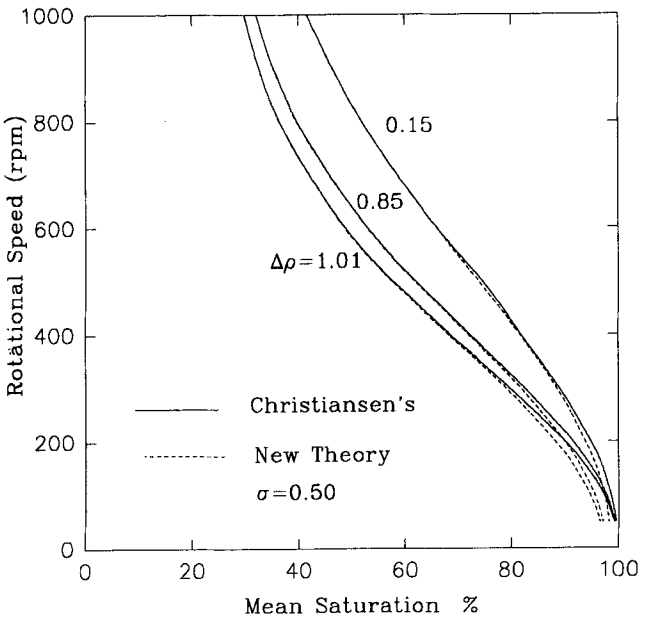

Figure 11. Production histories generated with two theories.

fluence for the applications mentioned, and leads to inaccurate capillary pressure information. The possible remedial measures may include: (1) initializing an experiment at a relatively high speed, say over 500 rpm, while concurrently losing detailed information in the high saturation zone (information near the threshold pressure); (2) omitting low-speed data points; (3) interpreting such data sets using the model developed in this article, which may complicate numerical calculations; and (4) developing a rotor with a new configuration that minimizes this effect (the main idea is to adopt a pivoted or tilted rotor head, which more closely aligns the gravitational and centrifugal fields, thereby reducing this effect). Because of the gravity degradation effect, centrifuge experiments for other purposes, such as relative permeability measurements (O'Meara et al., 1985) and oil recovery flooding processes (Nikakhtar et al., 1993), should also be carefully treated in order to obtain accurate information. A study is being carried out at the University of Manitoba to investigate the final remedial measure (Chen and Ruth, 1994). Also new data interpretation techniques are being explored (the third remedial measure) to improve the quality of capillary pressure curves.

Conclusions

A new three-dimensional centrifuge theory for capillary pressure data was constructed to consider all of the acting forces, especially gravitational acceleration. This latter force becomes pronounced for low speed experiments ($\omega < 500$ rpm). Numerical quantification shows that for speeds below 500 rpm, gravity alters the centrifugal field. If this alteration is not accounted for, the result will be inaccurate capillary pressure information at high saturation, near the threshold pressure.

Acknowledgment

The authors would like to thank ESSO Resources and NSERC for financial support for this project.

Notation

$A(r_0)$ = equipotential surface area, cm^2
C = constant defined in Eq. 4
C_g = characteristic factor, $C_g = (2g/\omega^2)$, cm
g = gravity acceleration, g/cm^2
H = height of slab-shaped core samples
I = point defined in Figure 1
J = point defined in Figure 1
K = point defined in Figure 1
P = potential
P_c = capillary pressure
P_{c1} = maximum capillary pressure at the reference point r_{inlet}
P_{cI} = capillary pressure at the point I
P_{cJ} = capillary pressure at the point J
P_{cK} = capillary pressure at the point K
P_t = threshold capillary pressure in Bentsen's model, Eq. 17
r = rotation radius, cm
r_0 = reference rotation radius, cm
r_{inlet} = inner endface radius of rotation, cm
r_{outlet} = bottom endface radius of rotation, cm
$r_{0\max}$ = maximum reference rotation radius, cm
$r_{0\min}$ = minimum reference rotation radius, cm
R = radius of core cylinder plug, cm
S_w = wetting-phase saturation
S_{wr} = irreducible connate wetting-phase saturation
$\bar{S}_w$ = mean wetting-phase saturation
V = volume of core-sample plug, cm^3
$\bar{V}$ = produced volume, cm^3
x = variable
y = variable
z = variable
z_0 = variable corresponding to r_0

Greek letters

α = characteristic angle defined in Eq. 1
θ = variable defined in the two-dimensional case in the Appendix
$\Delta\rho$ = density difference of fluid pairs
σ = pressure span in Bentsen's model, Eq. 17, psi
ω = angular rotation speed, rpm $\times (2\pi/60)$

Literature Cited

Ayappa, K. G., H. T. Davis, E. A. Davis, and J. Gordon, "Capillary Pressure: Centrifuge Method Revisited," *AIChE J.*, **35**, 365 (1989).

Bentsen, R. G., and J. Anli, "Using Parameter Estimation Techniques to Convert Centrifuge Data Into a Capillary-Pressure Curve," *Soc. Pet. Eng. J.*, **17**, 57 (1977).

Chen, Z. A., and D. W. Ruth, "Centrifugal Analysis of Pivoted Rotor System for Capillary Pressure Measurements," paper presented at the 45th Annual CIM Tech. Meet. of the Petroleum Society of CIM, Calgary, Alberta, Canada (June 12–15, 1994).

Christiansen, R. L., and K. S. Cerise, "Capillary Pressure: Reduction of Centrifuge Data," AIChE Meet., New York (Nov. 15–20, 1987).

Christiansen, R. L., "Geometric Concerns for Accurate Measurement of Capillary Pressure Relationships With Centrifuge Methods," *SPE Form. Eval.*, **7**, 311 (1992).

Corey, A. T., "The Interrelation Between Gas and Oil Relative Permeabilities," *Prod. Mon.*, 38 (Nov., 1954).

Forbes, P. L., Z. A. Chen, and D. W. Ruth, "Quantitative Analysis of Radial Effects on Centrifuge Capillary Pressure Curves," *SPE Form. Eval.*, submitted (1994).

Golaz, P., and R. G. Bentsen, "On the Use of the Centrifuge to Obtain Capillary Pressure Data," paper CIM Tech. Meeting, Calgary, Alberta, Canada (May 25–28, 1980).

Hassler, G. L., and E. Brunner, "Measurement of Capillary Pressures in Small Samples," *Pet. Trans., AIME*, **160**, 114 (1945).

Li, S.-J., *Engineering Fluid Mechanics*, Northwestern Univ. of Technology Press, Shenyang, P.R. China (1990).
Maron, M. J., *Numerical Analysis: A Practical Approach*, Macmillan, New York (1982).
Nikakhtar, B., A. Kantzas, P. de Witt, M. Pow, and A. George, "On the Characterization of Rock/Fluid and Fluid/Fluid Interactions in Carbonate Rocks Using the Ultracentrifuge," Meeting of AGM of CIM/ATM of Pet. Soc. of CIM, Calgary, Alberta, Canada (May 9–12, 1993).
O'Meara, D. J., Jr., and J. G. Crump, "Measuring Capillary Pressure and Relative Permeability in a Single Centrifuge Experiment," SPE Tech. Meeting and Exhibition, Las Vegas, NV (Sept. 22–25, 1985).
Ruth, D. W., and S. Wong, "Centrifuge Capillary Pressure Curves," *J. Can. Pet. Technol.*, **29**, 67 (1990).
Ruth, D. W., and Z. A. Chen, "On the Measurement and Interpretation of Centrifuge Capillary Pressure Curves: The SCA Survey Data," *The Log Analyst*, in press (1995).
Stroud, A. H., and D. Secrest, *Gaussian Quadrature Formulas*, Prentice-Hall, Englewood Cliffs, NJ (1966).
Thomeer, J. H. M., "Introduction of a Pore Geometrical Factor Defined by the Capillary Pressure Curves," *Pet. Trans. AIME*, **219**, 354 (1960).
Thomas, G. B., Jr., "Multiple Integrals," *Calculus and Analytical Geometry*, 3rd ed., Chap. 15, Addison-Wesley, Reading, MA (1960).

Appendix

Two-dimensional models

As shown in Figure 2a, if the core-sample plus is viewed from the top, we have an equation to describe a cross section of the core-plug cylinder to the X direction:

$$y^2 + z^2 = R^2 \tag{A1}$$

or

$$z = \pm\sqrt{R^2 - y^2}\,. \tag{A2}$$

Considering one-fourth of the cylinder, the area of the equipressure surface $A(r)$ will be

$$A(r) = 4\int_{\theta_1}^{\theta_2} zr\,d\theta = 4\int_{\theta_1}^{\theta_2}\sqrt{R^2 - y^2}\,r\,d\theta$$

$$= 4\int_{\theta_1}^{\theta_2}\sqrt{R^2 - r^2\sin^2\theta}\,r\,d\theta \tag{A3}$$

where $y = r\sin\theta$. The definition of θ can be found in the original publication (Christiansen, 1992).

In order to define integration limits for the preceding expression, we have to divide the internal cross-sectional area of the core plug into three zones: $r_{\text{inlet}} \le r \le \sqrt{r_{\text{inlet}}^2 + R^2}$, $\theta_1 = 0$, and $\theta_2 = \cos^{-1}(r_{\text{inlet}}/r)$ for zone 1; $r_{\text{inlet}} \le r \le r_{\text{outlet}}$, $\theta_1 = 0$, and $\theta_2 = \sin^{-1}(R/r)$ for zone 2; and $r_{\text{outlet}} \le r \le \sqrt{R^2 + r_{\text{outlet}}^2}$, $\theta_1 = \cos^{-1}(r_{\text{outlet}}/r)$ and $\theta_2 = \sin^{-1}(R/r)$ for zone 3.

For a slab-shaped core sample of height H along the axis of rotation, of width $2R$, in the direction of rotation, and with ends at distances r_{inlet} and r_{outlet} from the axis of rotation, it is not difficult to show that $r_{0\min} = r_{\text{inlet}}$, $r_{0\max} = \sqrt{r_{\text{outlet}}^2 + R^2}$, and the equipressure surface areas are given by

$$A(r) = 2Hr[\theta_2(r) - \theta_1(r)] \tag{A4}$$

where $\theta_1(r)$ and $\theta_2(r)$ are defined in the same way as in Christiansen's cylinder core samples, which cover three integration zones.

The boundary conditions of capillary pressure generally should be replaced by

$$P_c = 0 \qquad \text{at} \quad r_{0\max} \tag{A5}$$

and at $r_{\min}$ by

$$P_{c1} = \frac{1}{2}\Delta\rho\omega^2(r_{0\max}^2 - r_{0\min}^2). \tag{A6}$$

Then the capillary pressure at r will be

$$P_c = \frac{1}{2}\Delta\rho\omega^2(r_{0\max}^2 - r^2). \tag{A7}$$

For a cylindrical sample, $P_c = 0$ is imposed at the two points on the r_{outlet} face that lie in a common rotation plane at a distance $\sqrt{r_{\text{outlet}}^2 + R^2}$ from the axis of rotation. Pressure P_{c1} occurs at the center vertical line of the r_{inlet} face of the sample.

In the case of the slab sample, $P_c = 0$ on the two vertical edges of the r_{outlet} face. Pressure P_{c1} also occurs along a vertical line on the center of the r_{inlet} face. This line is parallel to the axis of rotation.

Three-dimensional model

Using the concept of equipotential surfaces, the material balance equation (volume balance) (Eq. 4) can be written as

$$\bar{S}_w = \frac{1}{V}\int_{r_{0\min}}^{r_{0\max}} S_w A(r_0)\,dx \tag{A8}$$

where $r_{0\min}$ and $r_{0\max}$ are the minimum and maximum distances that characterize the intersecting process of the two solids of revolution, shown in Figure 3.

The integral boundary for the problem is difficult to define, because it depends on different combinations of the parameters involved (C_g, R, r_{inlet}, and r_{outlet}). Generally, three cases must be considered: $C_g \le R$, $R \le C_g \le 2R$, and $C_g \le 2R$.

When $C_g \le R$, five different integration zones are observed, corresponding to five fluid volumes ($S_w = \Sigma V_{wi}/V$, $i = 1, 2, 3, 4, 5$, and S_w is the total mean saturation of the core sample).

For zone 1

$$V_{w1} = \int_{r_{\text{inlet}}}^{\sqrt{r_{\text{inlet}}^2 + 2RC_g}} S_w A_1(x)\,dx \tag{A9}$$

or

$$V_{w1} = \int_{r_{\text{inlet}}}^{\sqrt{r_{\text{inlet}}^2 + 2RC_g}} \int_{-\sqrt{R^2 - z_{m1}^2}}^{\sqrt{R^2 - z_{m1}^2}} \int_{R + (y^2 - x^2 + r_{\text{inlet}}^2)/C_g}^{\sqrt{R^2 - y^2}} \times S_w F(x, y, z)\,dz\,dy\,dx \tag{A10}$$

where

$$z_{m1} = \frac{-C_g + \sqrt{C_g^2 + 4\left(R^2 + r_{\text{inlet}}^2 + RC_g - x^2\right)}}{2}$$

is the upper junction point of the paraboloid and the cylinder at the inlet endface r_{inlet}, and $F(x, y, z)$ is defined in Eq. 9.

For zone 2

$$V_{w2} = \int_{\sqrt{r_{\text{inlet}}^2 + 2RC_g}}^{\sqrt{R^2 + r_{\text{inlet}}^2 + RC_g + C_g^2/4}} S_w A_2(x)\, dx. \quad \text{(A11)}$$

However, this equation has to be subdivided into several integrals

$$V_{w2} = 2\int_{\sqrt{r_{\text{inlet}}^2 + 2RC_g}}^{\sqrt{R^2 + r_{\text{inlet}}^2 + RC_g}} \int_0^{\sqrt{R^2 - z_{m2}^2}} \int_{-\sqrt{R^2 - y^2}}^{\sqrt{R^2 - y^2}} \times S_w f(x, y, z) dz\, dy\, dx$$

$$+2\int_{\sqrt{r_{\text{inlet}}^2 + 2RC_g}}^{\sqrt{R^2 + r_{\text{inlet}}^2 + RC_g}} \int_{\sqrt{R^2 - z_{m2}^2}}^{\sqrt{R^2 - z_{m1}^2}} \int_{\sqrt{R + (y^2 - x^2 - r_{\text{inlet}}^2)/C_g}}^{\sqrt{R^2 - y^2}} \times S_w f(x, y, z)\, dz\, dy\, dx$$

$$+2\int_{\sqrt{R^2 + RC_g + r_{\text{inlet}}^2}}^{\sqrt{R^2 + r_{\text{inlet}}^2 + RC_g + C_g^2/4}} \int_0^{\sqrt{R^2 - z_{m2}^2}} \int_{-\sqrt{R^2 - y^2}}^{\sqrt{R^2 - y^2}} \times S_w f(x, y, z)\, dz\, dy\, dx$$

$$+2\int_{\sqrt{R^2 + RC_g + r_{\text{inlet}}^2}}^{\sqrt{R^2 + r_{\text{inlet}}^2 + RC_g + C_g^2/4}} \int_{\sqrt{R^2 - z_{m2}^2}}^{\sqrt{R^2 - z_{m1}^2}} \int_{R + \frac{y^2 - x^2 - r_{\text{inlet}}^2}{C_g}}^{\sqrt{R^2 - y^2}} \times S_w f(x, y, z)\, dz\, dy\, dx$$

$$+4\int_{\sqrt{R^2 + RC_g + r_{\text{inlet}}^2}}^{\sqrt{R^2 + r_{\text{inlet}}^2 + RC_g + C_g^2/4}} \int_{\sqrt{R^2 - z_{m1}^2}}^{R} \int_0^{\sqrt{R^2 - y^2}} \times S_w f(x, y, z)\, dz\, dy\, dx \quad \text{(A12)}$$

where z_{m1} and z_{m2} are the upper and lower junction points at r_{inlet},

$$z_{m1} = \frac{-C_g + \sqrt{C_g^2 + 4\left(R^2 + r_{\text{inlet}}^2 + RC_g - x^2\right)}}{2},$$

and

$$z_{m2} = \frac{-C_g - \sqrt{C_g^2 + 4\left(R^2 + r_{\text{inlet}}^2 + RC_g - x^2\right)}}{2}.$$

For zone 3. It is quite simple to conduct the integration

$$V_{w3} = \int_{\sqrt{R^2 + r_{\text{inlet}}^2 + RC_g + C_g^2/4}}^{r_{\text{outlet}}} S_w A_3(x)\, dx \quad \text{(A13)}$$

or

$$V_{w3} = \int_{\sqrt{R^2 + r_{\text{inlet}}^2 + RC_g + C_g^2/4}}^{r_{\text{outlet}}} \int_{-R}^{R} \int_{-\sqrt{R^2 - y^2}}^{\sqrt{R^2 - y^2}} \times S_w f(x, y, z)\, dz\, dy\, dx. \quad \text{(A14)}$$

For zone 4. Here we have

$$V_{w4} = \int_{r_{\text{outlet}}}^{\sqrt{r_{\text{outlet}}^2 + 2RC_g}} S_w A_4(x)\, dx \quad \text{(A15)}$$

or

$$V_{w4} = 2\int_{r_{\text{outlet}}}^{\sqrt{r_{\text{outlet}}^2 + 2RC_g}} \int_0^{\sqrt{R^2 - z_{n1}^2}} \int_{-\sqrt{R^2 - y^2}}^{R + (y^2 - x^2 - r_{\text{outlet}}^2)/C_g} \times S_w f(x, y, z)\, dz\, dy\, dx$$

$$+2\int_{r_{\text{outlet}}}^{\sqrt{r_{\text{outlet}}^2 + 2RC_g}} \int_{\sqrt{R^2 - z_{n1}^2}}^{R} \int_{-\sqrt{R^2 - y^2}}^{\sqrt{R^2 - y^2}} \times S_w f(x, y, z)\, dz\, dy\, dx. \quad \text{(A16)}$$

For zone 5. The integral is complicated

$$V_{w5} = \int_{\sqrt{r_{\text{outlet}}^2 + 2RC_g}}^{\sqrt{R^2 + r_{\text{outlet}}^2 + RC_g + C_g^2/4}} S_w A_5(x)\, dx. \quad \text{(A17)}$$

This integral has to be subdivided to obtain

$$V_{w5} = 2\int_{\sqrt{r_{\text{outlet}}^2 + 2RC_g}}^{\sqrt{R^2 + r_{\text{outlet}}^2 + RC_g}} \int_{\sqrt{R^2 - z_{n2}^2}}^{\sqrt{R^2 - z_{n1}^2}} \int_{-\sqrt{R^2 - y^2}}^{R + (y^2 - x^2 + r_{\text{outlet}}^2)/C_g} \times S_w f(x, y, z)\, dz\, dy\, dx$$

$$+4\int_{\sqrt{r_{\text{outlet}}^2 + 2RC_g}}^{\sqrt{R^2 + r_{\text{outlet}}^2 - RC_g}} \int_{\sqrt{R^2 - z_{n1}^2}}^{R} \int_0^{\sqrt{R^2 - y^2}} \times S_w f(x, y, z)\, dz\, dy\, dx$$

$$+2\int_{\sqrt{r_{\text{outlet}}^2 - RC_g + r_{\text{inlet}}^2}}^{\sqrt{R^2 + r_{\text{outlet}}^2 + RC_g + C_g^2/4}} \int_{\sqrt{R^2 - z_{n2}^2}}^{\sqrt{R^2 - z_{n1}^2}} \times \int_{-\sqrt{R^2 - y^2}}^{R + (y^2 - x^2 - r_{\text{outlet}}^2)/C_g} S_w f(x, y, z)\, dz\, dy\, dx. \quad \text{(A18)}$$

where z_{n1} and z_{n2} are the upper and lower junction points at r_{outlet},

$$z_{n1} = \frac{-C_g + \sqrt{C_g^2 + 4\left(R^2 + r_{\text{outlet}}^2 + RC_g - x^2\right)}}{2},$$

and

$$z_{n2} = \frac{-C_g - \sqrt{C_g^2 + 4\left(R^2 + r_{\text{outlet}}^2 + RC_g - x^2\right)}}{2}.$$

When $C_g = 0$, zone 1 and zone 4 disappear. The equations will be reduced to

$$V_{w2} = 2\int_{r_{\text{inlet}}}^{\sqrt{R^2 + r_{\text{inlet}}^2}} \int_0^{\sqrt{R^2 - z_{m2}^2}} \int_{-\sqrt{R^2 - y^2}}^{\sqrt{R^2 - y^2}} \times S_w f(x, y, z)\, dz\, dy\, dx \quad \text{(A19)}$$

$$V_{w3} = \int_{\sqrt{R^2 + r_{\text{inlet}}^2}}^{r_2} \int_{-R}^{R} \int_{-\sqrt{R^2 - y^2}}^{\sqrt{R^2 - y^2}} \times S_w f(x, y, z)\, dz\, dy\, dx \quad \text{(A20)}$$

$$V_{w5} = 4\int_{\sqrt{r^{\text{outlet}}}}^{\sqrt{R^2 + r_{\text{outlet}}^2}} \int_{\sqrt{R^2 - z_{n1}^2}}^{R} \int_0^{\sqrt{R^2 - y^2}} \times S_w f(x, y, z)\, dz\, dy\, dx \quad \text{(A21)}$$

where $z_{m1} = z_{m2} = \pm\sqrt{R^2 - r_{\text{inlet}}^2 - x^2}$, and $z_{n1} = z_{n2} = \pm\sqrt{R^2 + r_{\text{outlet}}^2 - x^2}$. Therefore, $C_g = 0$ recovers Christiansen's two-dimensional case, which considers only the centrifugal force distribution inside the core sample due to nonradial considerations.

When $R \le C_g \le 2R$, the various integrals must be broken up before they are performed.

For zone 1,

$$V_{w1} = 2\int_{r_{\text{inlet}}}^{\sqrt{r_{\text{inlet}}^2 + RC_g + R^2}} \int_0^{\sqrt{R^2 - z_{m1}^2}} \int_{R + (y^2 - x^2 + r_{\text{inlet}}^2)/C_g}^{\sqrt{R^2 - y^2}} \times S_w f(x, y, z)\, dz\, dy\, dx$$

$$+ 2\int_{\sqrt{r_{\text{inlet}}^2 + RC_g + R^2}}^{\sqrt{r_{\text{inlet}}^2 + 2RC_g}} \int_0^{\sqrt{R^2 - z_{m1}^2}} \int_{R + (y^2 - x^2 + r_{\text{inlet}}^2)/C_g}^{\sqrt{R^2 - y^2}} \times S_w f(x, y, z)\, dz\, dy\, dx$$

$$+ 2\int_{\sqrt{r_{\text{inlet}}^2 + RC_g + R^2}}^{\sqrt{r_{\text{inlet}}^2 + 2RC_g}} \int_{\sqrt{R^2 - z_{m1}^2}}^{R} \int_{-\sqrt{R^2 - y^2}}^{\sqrt{R^2 - y^2}} \times S_w f(x, y, z)\, dz\, dy\, dx. \quad \text{(A22)}$$

For zone 2

$$V_{w2} = 2\int_{\sqrt{r_{\text{inlet}}^2 + 2RC_g}}^{\sqrt{R^2 + r_{\text{inlet}}^2 + RC_g + C_g^2/4}} \int_0^{\sqrt{R^2 - z_{m2}^2}} \int_{-\sqrt{R^2 - y^2}}^{\sqrt{R^2 - y^2}} \times S_w f(x, y, z)\, dz\, dy\, dx$$

$$+ 2\int_{\sqrt{r_{\text{inlet}}^2 + 2RC_g}}^{\sqrt{R^2 + r_{\text{inlet}}^2 + RC_g C_g^2/4}} \int_{\sqrt{R^2 - z_{m2}^2}}^{\sqrt{R^2 - z_{m1}^2}} \times \int_{R + (y^2 - x^2 + r_{\text{inlet}}^2)C_g}^{\sqrt{R^2 - y^2}} S_w f(x, y, z)\, dz\, dy\, dx$$

$$+ 2\int_{\sqrt{r_{\text{inlet}}^2 + 2RC_g}}^{\sqrt{R^2 + r_{\text{inlet}}^2 + RC_g + C_g^2/4}} \int_{\sqrt{R^2 - z_{m1}^2}}^{R} \int_{-\sqrt{R^2 - y^2}}^{\sqrt{R^2 - y^2}} \times S_w f(x, y, z)\, dz\, dy\, dx. \quad \text{(A23)}$$

For zone 4

$$V_{w4} = 2\int_{r_{\text{outlet}}}^{\sqrt{r_{\text{outlet}}^2 + RC_g + R^2}} \int_0^{\sqrt{R^2 - z_{n1}^2}} \int_{-\sqrt{R^2 - y^2}}^{R + (y^2 - x^2 + r_{\text{outlet}}^2)/C_g} \times S_w f(x, y, z)\, dz\, dy\, dx$$

$$+ 2\int_{r_{\text{outlet}}}^{\sqrt{r_{\text{outlet}}^2 + RC_g + R^2}} \int_{\sqrt{R^2 - z_{n1}^2}}^{R} \int_{-\sqrt{R^2 - y^2}}^{\sqrt{R^2 - y^2}} \times S_w f(x, y, z)\, dz\, dy\, dx$$

$$+ 2\int_{\sqrt{r_{\text{outlet}}^2 + RC_g + R^2}}^{\sqrt{r_{\text{outlet}}^2 + 2RC_g}} \int_0^{\sqrt{R^2 - z_{n1}^2}} \int_{-\sqrt{R^2 - y^2}}^{R + (y^2 - x^2 + r_{\text{outlet}}^2)/C_g} \times S_w f(x, y, z)\, dz\, dy\, dx. \quad \text{(A24)}$$

For zone 5

$$V_{w5} = 2\int_{\sqrt{r_{\text{outlet}} + 2RC_g}}^{\sqrt{R^2 + r_{\text{outlet}}^2 + RC_g + C_g^2/4}} \int_{\sqrt{R^2 - z_{n2}^2}}^{\sqrt{R^2 - z_{n1}^2}} \times \int_{-\sqrt{R^2 - y^2}}^{R + (y^2 - x^2 + r_{\text{outlet}}^2)/C_g} S_w f(x, y, z)\, dz\, dy\, dx. \quad \text{(A25)}$$

When $C_g \ge R$, a different set of integrals must be specified for this case.

For zone 1

$$V_{w1} = 2\int_{r_{\text{inlet}}}^{\sqrt{r_{\text{inlet}}^2 + RC_g + R^2}} \int_0^{\sqrt{R^2 - z_{m1}^2}} \int_{R + (y^2 - x^2 + r_{\text{inlet}}^2)/C_g}^{\sqrt{R^2 - y^2}} \times S_w f(x, y, z)\, dz\, dy\, dx$$

$$+ 2\int_{\sqrt{r_{\text{inlet}}^2 + RC_g + R^2}}^{\sqrt{r_{\text{inlet}}^2 + 2RC_g}} \int_0^{\sqrt{R^2 - z_{m1}^2}} \int_{R + (y^2 - x^2 + r_{\text{inlet}}^2)/C_g}^{\sqrt{R^2 - y^2}} \times S_w f(x, y, z)\, dz\, dy\, dx$$

$$+ 2\int_{\sqrt{r_{\text{inlet}}^2 + RC_g + R^2}}^{\sqrt{r_{\text{inlet}}^2 + 2RC_g}} \int_{\sqrt{R^2 - z_{m1}^2}}^{R} \int_{-\sqrt{R^2 - y^2}}^{\sqrt{R^2 - y^2}} \times S_w f(x, y, z)\, dz\, dy\, dx. \quad \text{(A26)}$$

For zone 2

$$V_{w2} = \int_{\sqrt{r_{\text{inlet}}^2 + 2RC_g}}^{r_{\text{outlet}}} \int_{-R}^{R} \int_{-\sqrt{R^2 - y^2}}^{\sqrt{R^2 - y^2}} S_w f(x, y, z)\, dz\, dy\, dx. \tag{A27}$$

For zone 3

$$V_{w3} = 2\int_{r_{\text{outlet}}}^{\sqrt{r_{\text{outlet}}^2 + RC_g + R^2}} \int_{0}^{\sqrt{R^2 - z_{n1}^2}} \int_{-\sqrt{R^2 - y^2}}^{R + (y^2 - x^2 + r_{\text{outlet}}^2)/C_g} \times S_w f(x, y, z)\, dz\, dy\, dx$$

$$+ 2\int_{r_{\text{outlet}}}^{\sqrt{r_{\text{outlet}}^2 + RC_g + R^2}} \int_{\sqrt{R^2 - z_{n1}^2}}^{R} \int_{-\sqrt{R^2 - y^2}}^{\sqrt{R^2 - y^2}} \times S_w f(x, y, z)\, dz\, dy\, dx$$

$$+ 2\int_{\sqrt{r_{\text{outlet}}^2 + RC_g + R^2}}^{\sqrt{r_{\text{outlet}}^2 + 2RC_g}} \int_{0}^{\sqrt{R^2 - z_{n1}^2}} \int_{-\sqrt{R^2 - y^2}}^{R + (y^2 - x^2 + r_{\text{outlet}}^2)/C_g} \times S_w f(x, y, z)\, dz\, dy\, dx. \tag{A28}$$

As a test, if we assume that the integrands in the preceding equations are unity, the results obtained should be equal to the volume of the core sample cylinder regardless of the C_g value. For a typical case, we take $R = 1.27$ cm, $r_{\text{inlet}} = 6.06$ cm, and $r_{\text{outlet}} = 8.6$ cm (1-in.-long core sample plug). Then the volume of the sample plug should be $\pi R^2(r_{\text{outlet}} - r_{\text{inlet}}) = 12.87037$ cm^3. We calculated the volume of the core plug for a wide range of C_g, and the volume values for all cases are almost the same as the true value $\pi R^2(r_{\text{outlet}} - r_{\text{inlet}})$. The relative percentage errors are all within 0.01, and the relative ratios of the calculated and actual volumes are between 0.998 and 1.005.

Manuscript received Oct. 15, 1993, and revision received Apr. 12, 1994.